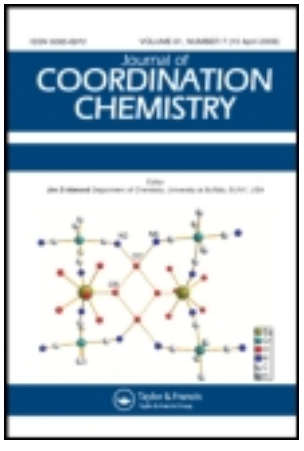

Journal of Coordination Chemistry
Publication details, including instructions for authors and subscription information:
http://www.tandfonline.com/loi/gcoo20

Spectroscopy, structure, and electrochemistry of transition metal complexes having $[M_2N_2OS_2]$ coordination sphere

Naveen V. Kulkarni [a], Gurunath S. Kurdekar [a], Srinivasa Budagumpi [a] & Vidyanand K. Revankar [a]
[a] Department of Studies in Chemistry, Karnatak University, Pavatenagar, Dharwad-580 003, Karnataka, India
Published online: 19 Aug 2010.

To cite this article: Naveen V. Kulkarni , Gurunath S. Kurdekar , Srinivasa Budagumpi & Vidyanand K. Revankar (2010): Spectroscopy, structure, and electrochemistry of transition metal complexes having $[M_2N_2OS_2]$ coordination sphere, Journal of Coordination Chemistry, 63:18, 3301-3312

To link to this article: http://dx.doi.org/10.1080/00958972.2010.511201

Journal of Coordination Chemistry
Vol. 63, No. 18, 20 September 2010, 3301–3312

Taylor & Francis
Taylor & Francis Group

Spectroscopy, structure, and electrochemistry of transition metal complexes having $[M_2N_2OS_2]$ coordination sphere

NAVEEN V. KULKARNI, GURUNATH S. KURDEKAR, SRINIVASA BUDAGUMPI and VIDYANAND K. REVANKAR*

Department of Studies in Chemistry, Karnatak University, Pavatenagar, Dharwad – 580 003, Karnataka, India

(*Received 28 February 2010; in final form 9 June 2010*)

Binuclear transition metal complexes of bicompartmental SNONS donors were synthesized and characterized by various physico-chemical techniques. Two different precursors with chloromethyl/formyl functionality at the 2 and 6 positions of phenolate ring are used to construct the ligands. The quinoxaline scaffolds provide SN donors incorporated at the 2 and 6 positions. Copper and zinc complexes are square pyramidal, whereas nickel and cobalt complexes are octahedral. The influence of two metal centers in terms of cooperative effect on the electronic, magnetic, electrochemical, and structural properties was investigated.

Keywords: 2,6-Bis-(chloromethyl)-4-methylphenol; 2,6-Diformyl-4-methylphenol; 3-Hydrazinylquinoxaline-2-thione; Bicompartmental ligand; Electrochemistry

1. Introduction

Model systems which may mimic the active sites of metallobiomolecules have been an incentive for the development of chemistry of binuclear complexes. Binuclear systems may bind and activate small molecules or may be used to investigate the cooperative effect of two metal centers on electronic, magnetic, and redox properties [1, 2].

Suitably designed binuclear systems would provide new reactivity patterns and physical properties that could not be achieved with mononuclear complexes. The neighboring metal centers may cooperate in promoting reactions and electronic interactions, leading to diverse physical properties [3, 4].

The symmetric and asymmetric nature of a number of homobinuclear transition metal-derived metallobiosites [5] and the ability of the individual metal ions to have quite distinct roles in the functioning of metalloenzymes have led to the design of symmetric and asymmetric binucleating ligands, which make the binuclear complexes capable of acting as models for metallobiosites.

Phenol-based compartmental ligands of ''end-off'' type, possessing two chelating arms attached to 2 and 6 positions of phenolate ring, have been used to provide phenoxo-bridged binuclear core complexes, with option for varying exogenous

*Corresponding author. Email: vkrevankar@rediffmail.com

ISSN 0095-8972 print/ISSN 1029-0389 online
DOI: 10.1080/00958972.2010.511201

bridges [1, 2, 6]. Recent X-ray crystallographic studies have indicated that most bimetallic/binuclear biosites are asymmetric with respect to the donors about the metals, the nature of the metal ions, the coordination number, and the geometric arrangement of the donors [5]. Thus, the design of end-off compartmental ligands providing a discrete binuclear core is of particular interest.

Quinoxaline capable of providing sulfur and nitrogen donors has been incorporated at the 2 and 6 position of phenolate ring to construct bicompartmental ligands. The mode of attachment is different in two ligands in order to provide different size and flexibility for the bicompartmental SNONS cavity. Transition metal(II) chlorides are employed for the construction of binuclear complexes. The structure as well as electronic, magnetic, and redox properties of the prepared complexes are studied.

Several transition metal binuclear complexes with a wide variety of coordination spheres exist [7–10]. The structural and functional properties of these complexes depend on the size and flexibility of coordination cavity, as well as the nature of donors and the metal ion.

2. Experimental

2.1. *Reagents and apparatus*

The chemicals used were reagent grade. Purified solvents were used for the synthesis of ligands and complexes. Syntheses of 2,6-bis-(chloromethyl)-4-methylphenol [11], 2,6-diformyl-4-methylphenol [12], and quinoxaline-2,3-(1,4H)-dithione [13] was done according to the method described with slight modification. Isatin was purchased from Sigma Aldrich and the metal chlorides {$CoCl_2 \cdot 6H_2O$, $NiCl_2 \cdot 6H_2O$, $CuCl_2 \cdot 2H_2O$, and $ZnCl_2$} were used for complex formation. Elemental (C, H, N and S) analysis was carried out on a THERMO QUEST elemental analyzer. Metal and chloride estimations were done by following standard procedures [14]. The molar conductivity measurements in DMF were made on an ELICO-CM-82 conductivity bridge with conductivity cell having cell constant $0.51\,cm^{-1}$. The magnetic susceptibility measurements were made using a Faraday balance at room temperature using $Hg[Co(SCN)_4]$ as calibrant. ^1H NMR spectra were recorded in DMSO-d_6/$CDCl_3$ on a Bruker-300 MHz spectrometer at room temperature using TMS as internal reference. Infrared (IR) spectra were recorded in KBr using an Impact-410 Nicolet (USA) FT-IR spectrometer from 4000 to $400\,cm^{-1}$. Electronic spectra of the compounds in DMF were recorded on a Hitachi 150-20 spectrophotometer from 1000 to 200 nm. Cyclic voltammetric studies were performed at room temperature in oxygen-free DMF created by purging with pure nitrogen, using a CHI1110A Electrochemical analyzer (USA) comprising a three electrode assembly of glassy carbon working electrode, platinum auxiliary electrode, and non-aqueous Ag^+/AgCl reference electrode. Tetramethylammonium chloride ($0.01\,mol\,L^{-1}$) was used as supporting electrolyte and the instrument was standardized by ferrocene/ferrocenium redox couple. FAB mass spectra were recorded from a JEOL SX 102/DA-6000 mass spectrometer using argon/xenon (6 kV, 10 mA) as the FAB gas and 3-nitrobenzylalcohol as matrix. TG and DTA measurements were done in nitrogen on a Universal V2 4F TA instrument at the scanning rate of $10^\circ C\,min^{-1}$ from 25 to 1000°C.

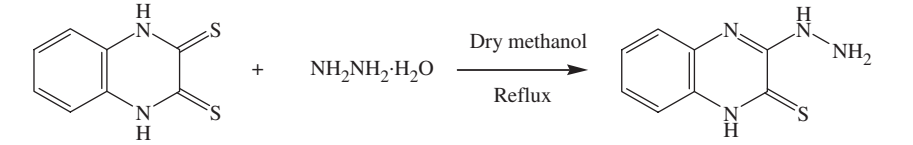

Quinoxaline-2,3(1,4H)-dithione Hydrazine hydrate 3-Hydrazinylquinoxaline-2(1H)-thione

Figure 1. Schematic representation of preparation of 3-hydrazinylquinoxaline-2-thione.

2.2. *Synthesis*

2.2.1. Synthesis of 3-hydrazinylquinoxaline-2(1H)-thione. Hydrazine hydrate in methanol (0.6 mL, 0.1 mol L^{-1}) was added dropwise to a methanolic solution of quinoxaline-2,3-(1,4H)-dithione (1.94 g, 0.1 mol L^{-1}) with constant stirring. The mixture was then refluxed for 2 h over a steam bath. Product formed as a shiny dark yellow solid was filtered, thoroughly washed with methanol and air dried (Yield: 83%, m.p.: 182–184°C) (figure 1).

2.2.2. Synthesis of HL^1 and HL^2. Hot methanolic solution of 3-hydrazinylquinoxaline-2(1H)-thione (1.92 g, 0.1 mol L^{-1}) was added dropwise to a stirring solution of 2,6-diformyl-4-methylphenol (0.82 g, 0.05 mol L^{-1}) (for HL^1)/2,6-bis-(chloromethyl)-4-methyl phenol (1.08 g, 0.05 mol L^{-1}) (for HL^2) in dry methanol. The mixture was refluxed for 2 h on a heating mantle and the solid separated was isolated by filtration. The solid was thoroughly washed with methanol and dried {(HL^1, m.p.: 169–172°C, Yield: 78%) (HL^2, m.p.: 173–176°C, Yield: 79%)}. The reaction pathway is given in figure 2.

2.2.3. Preparation of complexes. A solution of ligand HL^1 (0.524 g, 0.01 mol L^{-1}) in methanol was added to methanolic solution of $CuCl_2 \cdot 2H_2O$ (0.341 g, 0.002 mol L^{-1}) with constant stirring and refluxed on a heating mantle for 1 h. The copper complex, separated as greenish black solid, was filtered, washed thoroughly with methanol and dried.

Similar procedure was followed for the preparation of the other complexes with appropriate amounts of ligands and metal salts [{HL^1 (0.524 g, 0.01 mol L^{-1}), HL^2 (0.538 g, 0.01 mol L^{-1})}, {$CoCl_2 \cdot 6H_2O$ (0.475 g, 0.02 mol L^{-1}), $NiCl_2 \cdot 6H_2O$ (0.474 g, 0.02 mol L^{-1}), $CuCl_2 \cdot 2H_2O$ (0.341 g, 0.002 mol L^{-1}), and $ZnCl_2$ (0.271 g, 0.02 mol L^{-1})}].

3. Results and discussion

The phenoxo-bridged binuclear complexes obtained in the present investigation were non-hygroscopic, amorphous solids insoluble in ethanol, water, and chlorohydrocarbons, but soluble in DMF and DMSO. The composition and coordination geometry of these complexes have been established based on elemental analyses,

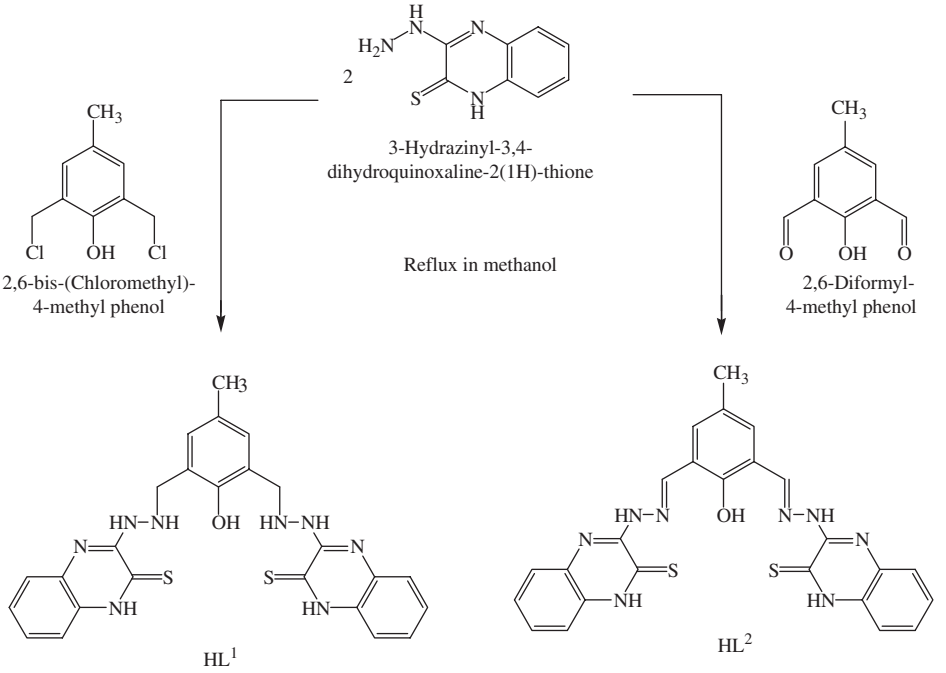

Figure 2. Schematic representation of synthesis of HL^1 and HL^2.

IR, NMR, mass spectral analyses, and TG studies. All the experimental results are in good agreement with the molecular formulae suggested for the compounds. The elemental analyses data of the ligands and their complexes along with molar conductivity values are compiled in table 1.

3.1. *Molar conductivity measurements*

The molar conductance values of the complexes measured at room temperature in DMSO solution with 10^{-3} mol dm^{-3} concentration are in the range 13.3–16.8 Ohm^{-1} cm^2 mol^{-1}, indicating non-electrolytic nature of the complexes [15].

3.2. *IR spectral studies*

Key IR absorption bands are summarized in table 2. Both ligands exhibit absorption bands of medium intensity in the 3100–3330 cm^{-1} region assigned to ν(NH) [16]. In spectra of complexes these bands shift to higher frequency and broaden in some complexes due to overlapping ν(OH) of coordinated water molecules at 3390–3450 cm^{-1}. The absorption due to phenolic ν(OH) is at 3050 cm^{-1} as a weak band, which disappears upon complexation, indicating deprotonation and coordination of phenoxide [17]. This is further supported by the shift of phenolic ν(C–O) at ~1300 cm^{-1} in ligands to higher frequency by 9–45 cm^{-1} in the spectra of complexes. The thioamide bands having a major contribution from C=S chromophore are

Table 1. Chemical composition and molar conductivity data of ligands and complexes.

Compound	Formula	Color	Melting/decomposition temperature (°C)	Yield in %	Elemental analysis (%) calculated (found)						Molar conductance Λ_M ($Ohm^{-1}\,cm^2\,mol^{-1}$)
					C	H	N	S	M	Cl	
HL^1	$[C_{25}H_{24}N_8S_2O]$	Orange yellow	169–172	89	58.13 (58.25)	4.65 (4.72)	21.70 (21.64)	12.40 (12.38)	–	–	–
CoL^1	$[Co_2L^1(\mu Cl)Cl_2(H_2O)_2]$	Brown	>300	84	38.70 (38.62)	3.48 (3.53)	14.45 (14.56)	8.25 (8.32)	15.17 (15.29)	13.74 (13.82)	16.8
NiL^1	$[Ni_2L^1(\mu Cl)Cl_2(H_2O)_2]$	Brown	>300	83	38.73 (38.80)	3.48 (3.56)	14.46 (14.35)	8.26 (8.32)	15.10 (15.04)	13.75 (13.68)	15.3
CuL^1	$[Cu_2L^1(\mu Cl)Cl_2]$	Greenish black	>300	82	40.08 (40.12)	3.07 (3.05)	14.96 (14.87)	8.55 (8.56)	16.96 (16.92)	14.22 (14.30)	14.2
ZnL^1	$[Zn_2L^1(\mu Cl)Cl_2]$	Orange	>300	80	39.86 (39.92)	3.05 (3.01)	14.88 (14.81)	8.50 (8.61)	17.40 (17.48)	14.15 (14.19)	13.3
HL^2	$[C_{25}H_{20}N_8S_2O]$	Yellow	173–176	87	59.76 (59.82)	3.98 (3.88)	22.31 (22.40)	12.74 (12.68)	–	–	–
CoL^2	$[Co_2L^2(\mu Cl)Cl_2(H_2O)_2]$	Brown	>300	81	38.91 (39.00)	2.98 (2.89)	14.82 (14.78)	8.30 (8.43)	15.25 (15.32)	13.81 (13.88)	13.9
NiL^2	$[Ni_2L^2(\mu Cl)Cl_2(H_2O)_2]$	Brown	>300	79	38.93 (38.97)	2.98 (2.97)	14.83 (14.88)	8.30 (8.43)	15.18 (15.26)	13.82 (13.91)	15.9
CuL^2	$[Cu_2L^2(\mu Cl)Cl_2]$	Greenish black	>300	80	40.29 (40.36)	2.55 (2.68)	15.04 (15.10)	8.59 (8.52)	17.05 (16.88)	14.30 (14.46)	14.2
ZnL^2	$[Zn_2L^2(\mu Cl)Cl_2]$	Yellow	>300	79	40.08 (40.00)	2.53 (2.59)	14.96 (15.03)	8.55 (8.63)	17.50 (17.62)	14.22 (14.31)	15.4

Table 2. IR spectral data in cm^{-1}.

Compound	ν(OH) water	ν(NH)	ν(C=N)	ν(C=N) ring	Thioamide bands		ν(C–O)
HL^1	–	3162m 3106m	–	1613s	1388s	858s	1300m
CoL^1	3421b	3200b	–	1614m	1350 w	830w	1326m
NiL^1	3446b	3200b	–	1617m	1345w	830w	1326m
CuL^1	–	3150b	–	1624m	1371m	840w	1320m
ZnL^1	–	3180b	–	1617s	1350w	835w	1321m
HL^2	–	3250b	1640s	1606s	1382s	850m	1302m
CoL^2	3399b	3291m	1631s	1540s	1377m	831m	1320m
NiL^2	3422b	3200b	1634m	1618s	1377m	830w	1309m
CuL^2	–	3327s	1638s	1551s	1370m	820m	1334s
ZnL^2	–	3333s	1626s	1578s	1388m	848m	1346m

s – strong absorption, m – medium, w – weak, and b – broad.

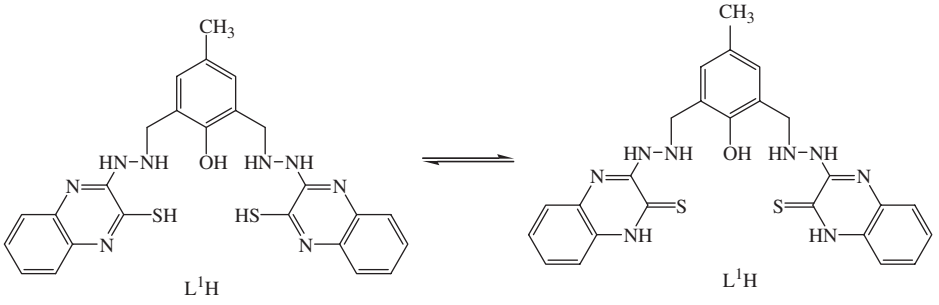

Figure 3. Thioketo-enol tautomerism in HL^1.

observed around 1385 and 855 cm^{-1} in ligands, which later reduce in intensity and shift to lower frequency upon complexation, suggesting the coordination of thione sulfur to metal [18]. For HL^2, a sharp band at 1640 cm^{-1} is assigned to ν(C=N) [19]. In the complexes it shifts to lower frequency region due to the azomethine nitrogen coordination [19]. Low-frequency non-ligand bands at 500–600 and 450–500 cm^{-1} are assigned to ν(M–N) and ν(M–S), respectively [18].

3.3. *^{1}H NMR studies*

NMR studies provide significant conclusion regarding the nature of bonding and coordination. Ligand HL^1 has a thio-enol tautomeric equilibrium in solution ($CDCl_3$) (figure 3), shown by the proton resonance at 4.61 ppm (D_2O exchangeable). But in the zinc complex spectrum, absence of this peak and appearance of a new broad peak at 11.50 ppm suggest the thioketo form and sulfur coordination [19]. The phenolic –OH observed at 8.40 ppm in the ligand (D_2O exchangeable) disappears upon complexation, indicating deprotonation and phenoxide coordination [17]. The peak at 7.89 ppm is attributed to hydrazine protons [18] and the peak at 3.61 is assigned to methylene amine protons, shifted downfield upon complexation. The aromatic protons are resonated in

Table 3. The electronic spectra and magnetic moment data.

Compound	λ_{max} in nm ($\sim\varepsilon$ in L cm^{-1} mol^{-1})	μ_{eff} (BM)
HL^1	250(10000), 280(9000), 320(9000), 330(8500)	–
CoL^1	321(9800), 350(1100), 425(25000), 530(110)	3.35
NiL^1	320(10100), 421(24000), 460(200), 650(150)	2.81
CuL^1	300(12000), 373(10000), 423(26000), 450(150), 546(100)	1.08
ZnL^1	280(12000), 350(1000), 400(1000), 420(23000)	Diamagnetic
HL^2	242(12000), 278(9000), 316(8500), 327(8500), 362(9200)	–
CoL^2	316(10000), 350(10000), 420(25000), 520(100)	3.31
NiL^2	340(9800), 420(25000), 471(250), 645(200)	2.80
CuL^2	300(9800), 360(8700), 420(23000), 440(130), 552(100)	1.06
ZnL^2	280(10000), 350(9800), 380(9500), 422(22000)	Diamagnetic

the range 6.50 to 7.60 ppm, methylene protons resonate at 2.25 ppm, and methyl protons of cresol absorb at 1.65 ppm [20]. In the proton NMR spectrum of ligand HL^2, broad peaks at 11.77 and 10.37 ppm (D_2O exchangeable) are attributed to the quinoxaline ring –NH and phenolic –OH, respectively. The azomethine protons resonate at 8.64 ppm and hydrazine NH at 7.70 ppm. The aromatic protons are observed at 6.60–7.49 ppm and methyl protons are at 2.25 ppm. The peak at 10.37 ppm corresponding to the phenolic –OH disappears in the zinc complex. All other protons shift downfield upon complexation.

3.4. *Electronic spectral studies*

Electronic spectral data are summarized in table 3. Ligands HL^1 and HL^2 exhibit similar spectral features in the UV-Vis region with peaks at 250, 280, and 320 nm, with molar absorptivity of $\varepsilon \sim 10{,}000$ L cm^{-1} mol^{-1}. The sharp intense peak at 250 nm assigned to intraligand π–π^* transition remains unaltered even after complexation. Absorption at 300–320 nm is assigned to n–π^* transition from phenoxide to aromatic π system (intraligand charge-transfer transition) [21]. The absorptions at 320–350 nm were assigned to the $n \rightarrow \pi^*$ transitions of the thioamide chromophore. HL^2 exhibits a broad peak at 350 nm corresponding to the $n \rightarrow \pi^*$ transition associated with azomethine [22]. On complexation, this peak shows red shift due to the donation of electrons to the metal through coordination [21]. All the complexes have an absorption peak at 350–380 nm ($\varepsilon \sim 10{,}000$ L cm^{-1} mol^{-1}), which is assigned to the charge-transfer transition from the filled pπ orbital of the bridging phenolic oxygen to the vacant d orbital of the metal [21]. An intense peak at 420 nm ($\varepsilon \sim 25{,}000$ L cm^{-1} mol^{-1}) is assigned to S$\rightarrow$M(II), ligand to metal charge-transfer transition (LMCT) [18]. The cobalt complexes have a medium intensity absorption in the visible region around 500 nm ($\varepsilon \sim 100$ L cm^{-1} mol^{-1}), assigned to d–d transition corresponding to $^4T_{1g} \rightarrow {}^4A_{2g}$, suggesting an octahedral geometry [23, 24]. The absorption corresponding to $^4T_{1g}(F) \rightarrow {}^4T_{1g}(P)$ transition is obscured due to the strong CT absorptions. The nickel(II) complexes exhibit many absorptions in the visible region with molar absorptivity in the range 60–80 L cm^{-1} mol^{-1}. Appearance of these spin-allowed transitions (around 460 and 650 nm) suggest an octahedral geometry with the absorptions assigned to $^3A_{2g} \rightarrow {}^3T_{1g}(P)$ and $^3A_{2g} \rightarrow {}^3T_{1g}$, respectively [25, 26]. Electronic spectra of copper complexes display a broad absorption at 500–650 nm

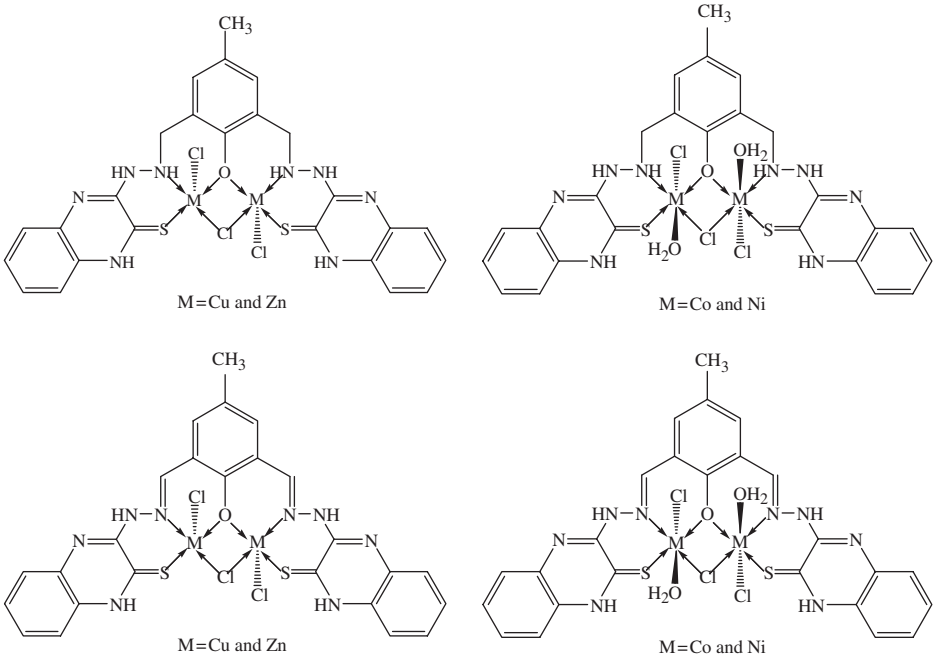

Figure 4. Proposed structures of complexes.

along with the intraligand and charge-transfer transitions. Because of the Jahn–Teller distortion and low symmetry environment around Cu(II), detailed interpretation is complicated [27]. The more intense charge transfer bands, which extend deep into the visible region, also prevent the analysis of d–d transitions in the complexes. Both the zinc complexes have shown a strong absorption peak around 370–400 nm, due to LMCT, along with intra-ligand transitions in the 280–320 nm range.

3.5. *Magnetochemistry*

Magnetic susceptibility measurements were done at room temperature (values given in table 3). The magnetic moments are found to be 3.35 and 3.31 BM for CoL^1 and CoL^2, 2.81 and 2.81 BM for NiL^1 and NiL^2, and 1.08 and 1.06 BM for CuL^1 and CuL^2, respectively. The subnormal values of magnetic moment are attributed to the spin exchange interaction between the closely spaced metal ions by phenoxide endogenous bridging [28, 29].

3.6. *FAB mass spectral studies*

The mass spectra of the complexes CuL^1 and CuL^2 exhibit intense peaks for the molecular ions at $m/z = 749$ and 744, respectively. The molecular ion peak corresponds to the mass of entire binuclear complex including bridged chloride and coordinated chloride ions. The general formula $[Cu_2L(\mu Cl)Cl_2]$ is hence assigned for both complexes, which agree well with elemental analysis data. The proposed structures of complexes are given in figure 4.

3.7. *TG-DTA analysis*

Thermal behaviors of CuL^1, NiL^1, CuL^2, and NiL^2 complexes were examined from 25 to 1000°C. The thermogram of CuL^1 shows a plateau region up to 230°C, indicating the absence of water in the complex. Disintegration takes place at 230–290°C with weight loss (15.81%) due to the removal of three chlorides as HCl. The exothermic nature of decomposition was indicated by the DTA curve. Further, gradual decomposition at higher temperature is assigned to ligand and the residue was CuO. For NiL^1, decomposition takes place in three steps. Weight loss (4.74%) at 50–120°C corresponds to the elimination of two water molecules. The corresponding DTA curve indicates the endothermic nature of the process. The second step of decomposition at 150–300°C was assigned to the loss of three chlorides as HCl (14.34%). Third step was the decomposition of ligand and the final product was NiO. CuL^2 decomposed in two steps corresponding to the loss of three chlorides (14.30% weight loss at 200–300°C) and the fragmentation of the ligand. Final decomposition product was copper oxide. NiL^2 has exhibited three-step decomposition as NiL^1, assigned to elimination of coordinated water (4.74% weight loss, 80–110°C), evolution of three chlorides (14.95% weight loss, ~225°C), and ligand decomposition.

3.8. *Electrochemistry*

The electrochemistry of oxo-bridged binuclear copper complexes is of interest because of the biological significance of the Cu(II)/Cu(I) redox couple. Studies reveal that copper electron transfer proteins and the mechanisms of copper enzymes are due to the ready accessibility of the Cu(I) oxidation state [30, 31]. Although the oxidation state +3 is unusual for copper, the existence of Cu(III) complexes as intermediates in various enzymatic and non-enzymatic reactions have raised interest in Cu(III) complexes in biological systems. To understand the electrochemistry of metallobiomolecules, studies on the electrochemical behavior of copper complexes are necessary [32]. The cyclic voltammetric study of molecules that contain two or more chemically equivalent electroactive sites is a point of attention. Cyclic voltammograms for molecules with multiple, non-interacting redox centers will be similar to those of the corresponding species with a single center, and ΔE_p will be 58 mV [33]; departure from this generalization may be due to electronic interactions between metal centers.

In binuclear copper(II) complex the sequential electron transfer processes are represented as

$$Cu^{II} - Cu^{II} \underset{E_1^f}{\overset{e^-}{\rightleftharpoons}} Cu^{II} - Cu^{II\mp I} \underset{E_2^f}{\overset{e^-}{\rightleftharpoons}} Cu^{II\mp I} - Cu^{II\mp I}$$

If for particular case $E_1^f \approx E_2^f$, the net result would be transfer of two electrons at a single potential [34, 35]. The redox behavior of binuclear copper(II) complexes can be interpreted by the consideration of the comproportionation constant, K_{com}, which relates mixed valence pair with native-valence system as follows:

$$Cu^{II} - Cu^{II} + Cu^{II\mp I} - Cu^{II\mp I} \overset{K_{com}}{\rightleftharpoons} 2Cu^{II} - Cu^{II\mp I}$$

$$\log K_{com} = \left(E_1^f - E_2^f/0.0591\right)$$

Table 4. Cyclic voltammetry data.

Compound	Scan rate ($V\,s^{-1}$)	Epa_1 (V)	Epa_2 (V)	Epc_2 (V)	Epc_1 (V)	ΔEp_1[a] (V)	ΔEp_2[b] (V)	$E_{1/2}(1)$[c] (V)	$E_{1/2}(2)$[d] (V)	Ipc_1/Ipa_1	Ipc_2/Ipa_2
CuL^1	0.15	0.20	0.50	0.34	0.02	0.18	0.16	0.11	0.42	0.88	0.87
	0.1	0.18	0.48	0.36	0.04	0.14	0.12	0.11	0.42	0.89	0.87
	0.05	0.16	0.46	0.38	0.06	0.10	0.08	0.11	0.42	0.92	0.88
CuL^2	0.15	0.12	0.52	0.33	0.03	0.09	0.21	0.07	0.43	0.91	0.88
	0.1	0.1	0.50	0.35	0.05	0.05	0.15	0.07	0.43	0.92	0.89
	0.05	0.08	0.48	0.37	0.07	0.01	0.09	0.07	0.43	0.94	0.9

[a] $\Delta Ep_1 = Epa_1 - Epc_1$.
[b] $\Delta Ep_2 = Epa_2 - Epc_2$.
[c] $E_{1/2}(1) = (Epa_1 + Epc_1)/2$.
[d] $E_{1/2}(2) = (Epa_2 - Epc_2)/2$.

If the mixed-valence species are unstable with respect to disproportionation, K_{com} tends to zero and $E_1^f \approx E_2^f$, which represent the two electron transfer at a single potential. But in other cases where mixed-valent species are stable, the cyclic voltammogram should give two successive reversible or quasireversible redox potentials. The stability of the mixed-valent species increases as the separation in potential between the two successive reduction or oxidation steps increases [36].

In the present work, copper complexes were investigated for electrochemical behavior in DMSO ($0.01\,mol\,L^{-1}$). The compounds were scanned from -1 to $+1\,V$ with three different scan rates (0.05, 0.1, and $0.15\,V\,s^{-1}$). The numerical data are presented in table 4 and representative voltammograms are provided in Supplementary material. In the case of CuL^1, during the anodic scan, two sequential oxidation peaks were observed at $Ea_1 = 0.16\,V$ and $Ea_2 = 0.48\,V$, representing the oxidation reactions. In the corresponding reverse scan (cathodic scan), two responses were observed at $Ec_1 = 0.36\,V$ and $Ec_2 = 0.04\,V$, representing the consequent reduction reactions. CuL^2 exhibits similar redox behavior with $Ea_1 = 0.10\,V$ and $Ea_2 = 0.50\,V$, and $Ec_1 = 0.35\,V$ and $Ec_2 = 0.05\,V$. The electrochemical responses exhibited by both complexes were purely metal based, since the corresponding ligands and zinc complexes are redox inactive. Hence, the two-step, two-electron redox process is assigned according to the sequence

$$Cu^{II} - Cu^{II} \underset{-e^-}{\overset{+e^-}{\rightleftharpoons}} Cu^{II} - Cu^{II\mp I} \underset{-e^-}{\overset{+e^-}{\rightleftharpoons}} Cu^{II\mp I} - Cu^{II\mp I}$$
$$E_1^o \qquad\qquad E_2^o$$

Although the chemical environment around the two metals in binuclear complexes is same, the overall two-electron exchanges appear as separate one-electron processes indicating that oxidation/reduction at one site induces steric and electronic influence on the other site, and hence induces a positive/negative shift to the oxidation/reduction potential of metal ion. The large difference between the redox potentials observed $\{[\Delta E = E_{1/2}(1) - E_{1/2}(2)] = 310$ and 360 mV, respectively, for CuL^1 and $CuL^2\}$ indicates considerable stability of the mixed-valence species ($K_{com} \sim 10^6$). In both complexes the redox processes are chemically quasireversible, as evidenced by the following criteria: (i) ΔE_p is greater than 59 mV, (ii) $Ip_a/Ip_c \sim 1$, and (iii) Ep_c shifts negatively with increasing scan rate. ΔE_p values of redox couples vary with scan rate and decrease

significantly with decrease in scan rate, indicating possible reversibility of redox reactions at slow rate. The appearance of Cu^{II}/Cu^{III} and the absence of Cu^{II}/Cu^{I} redox couple can be explained in terms of flexibility and size of the coordination cavity in the complexes and the geometric requirements and the size of the metal ions in different oxidation states. The reduction of Cu^{II} (d^9) to Cu^{I} (d^{10}) involves an increase in the metal radius and a configuration changes from square planar to tetrahedral. On the other hand, Cu^{III} (d^8) tends to assume square-planar coordination geometry with a low spin ground state and the oxidation of Cu^{II} to Cu^{III} involves reduction in ionic radius [37]. The constrained cavity fits Cu^{III} better and thus stabilizes the Cu^{III} complex. The extra stability achieved by the complex on oxidation will influence the redox reaction and slow the rate of reduction.

4. Conclusion

HL^1 and HL^2 are monobasic binucleating chelates and provide bicompartmental SNONS cavities which fit transition metal(II) ions. Copper and zinc complexes are square pyramidal, while nickel and cobalt complexes are octahedral. Chloride binds two metal ions as exogenous bridge. Mutual influence of two metal centers in terms of cooperative effect on the electronic, magnetic, and structural properties occur. The sequential two step redox processes exhibited by copper complexes are correlated to stereochemical arrangements. The differences of SNONS cavity in the two ligands have very little influence over electronic, magnetic, and electrochemical properties of complexes.

Acknowledgments

The authors thank Department of Chemistry and USIC, Karnatak University, Dharwad for providing spectral and analytical facility. Recording of FAB mass spectra (CDRI Lucknow) is gratefully acknowledged. The authors Naveen Kulkarni and Srinivasa Budagumpi thank Karnatak University, Dharwad and UGC, New Delhi for the Nilekani Scholarship and RFSMS.

References

[1] S.J. Smith, C.J. Noble, R.C. Palmer, G.R. Hanson, G. Schenk, L.R. Gahan, M.J. Riley. *J. Biol. Inorg. Chem.*, **13**, 499 (2008).
[2] L.M. Mirica, X. Ottenwaelder, T. Daniel, P. Stack. *Chem. Rev.*, **104**, 1013 (2004).
[3] A.L. Gavrilova, B. Bosnich. *Chem. Rev.*, **104**, 349 (2004).
[4] R. Than, A.A. Feldmann, B. Krebs. *Coord. Chem. Rev.*, **182**, 211 (1999).
[5] N. Mitic, S.J. Smith, A. Neves, L.W. Guddat, L.R. Gahan, G. Schenk. *Chem. Rev.*, **106**, 3338 (2006).
[6] A.D. Naik, S.M. Annigeri, U.B. Gangadharmath, V.K. Revankar, V.B. Mahale. *J. Mol. Struct.*, **616**, 119 (2002).
[7] C. Demetgul, M. Karakaplan, S. Serin, M. Digrak. *J. Coord. Chem.*, **62**, 3544 (2009).
[8] K.S. Bharathi, S. Sreedaran, P. Hema Priya, A.K. Rahiman, K. Rajesh, L. Jagadish, V. Kaviyarasan, V. Narayanan. *J. Coord. Chem.*, **62**, 1356 (2009).

[9] J. Sung, W.T. Hsu, A. Yeh, Y.J. Chen. *J. Coord. Chem.*, **61**, 2216 (2008).
[10] K.S. Bharathi, S. Sreedaran, R.A. Ayswarya, A.K. Rahiman, K. Rajesh, V. Narayanan. *J. Coord. Chem.*, **62**, 600 (2009).
[11] A.S. Borovik, V. Papaefthymiou, L.F. Taylor, O.P. Anderson, L. Que Jr. *J. Am. Chem. Soc.*, **111**, 6183 (1989).
[12] D.A. Denton, H. Suschitzky. *J. Chem. Soc.*, 4741 (1963).
[13] L.J. Theriot, K.K. Ganguli, S. Kavarnos, I. Bemal. *J. Inorg. Nucl. Chem.*, **31**, 3133 (1969).
[14] A.I. Vogel. *A Text book of Quantitative Inorganic Analysis*, 3rd Edn, Longmans Green, London (1961).
[15] W.J. Geary. *Coord. Chem. Rev.*, **7**, 81 (1971).
[16] S. Budagumpi, U.N. Shetti, N.V. Kulkarni, V.K. Revankar. *J. Coord. Chem.*, **62**, 3961 (2009).
[17] A.D. Naik, V.K. Revankar. *Proc. Indian Acad. Sci. (Chem. Sci.)*, **113**, 285 (2001).
[18] N.V. Kulkarni, G.S. Hegde, G.S. Kurdekar, S. Budagumpi, M.P. Sathisha, V.K. Revankar. *Spectrosc. Lett.*, **43**, 235 (2010).
[19] N.V. Kulkarni, M.P. Sathisha, S. Budagumpi, G.S. Kurdekar, V.K. Revankar. *J. Coord. Chem.*, **63**, 1451 (2010).
[20] A.D. Naik, S.M. Annigeri, U.B. Gangadharmath, V.K. Revankar, V.B. Mahale. *Spectrochim. Acta, Part A*, **58**, 1713 (2002).
[21] S.M. Annigeri, M.P. Sathisha, V.K. Revankar. *Transition Met. Chem.*, **32**, 81 (2007).
[22] A.B.P. Lever. *Inorganic Electronic Spectroscopy*, Elsevier, New York (1968).
[23] J.C. Bailar, H.J. Emeleus, S.R. Nyholm, A.F.T. Dickenson. *Comprehensive Inorganic Chemistry*, Vol. 3, Pergamon Press, New York (1975).
[24] A.S. El-Tabl, F.A. Aly, M.M.E. Shakdofa, A.M.E. Shakdofa. *J. Coord. Chem.*, **63**, 700 (2010).
[25] K. Nakamoto, P.J. McCarthy. *Spectroscopy and Structure of Metal Chelate Compounds*, John Wiley & Sons, New York (1968).
[26] K.S. Abou-Melha. *J. Coord. Chem.*, **61**, 2053 (2008).
[27] H. Okawa, M. Tadokoro, Y. Aratake, M. Ohba, K. Shindo, M. Mitsumi, M. Tomono, D.E. Funton. *J. Chem. Soc., Dalton Trans.*, 253 (1993).
[28] A.D. Naik, S.M. Annigeri, U.R. Gangadharmath, V.K. Revankar, V.B. Mahale, V.K. Reddy. *Bull. Chem. Soc. Jpn.*, **75**, 2161 (2002).
[29] R.A. Lal, S. Choudhury, A. Ahmed, M. Chakraborty, R. Borthakur, A. Kumar. *J. Coord. Chem.*, **62**, 3864 (2009).
[30] R.W. Hay, J.R. Dilworth, K.B. Nolan. *Perspectives on Bioinorganic Chemistry*, Vol. 1, JAI Press, London (1991).
[31] O. Farver, I. Pecht. *Coord. Chem. Rev.*, **84**, 17 (1989).
[32] D.A. Rocklife, A.E. Martell. *Inorg. Chem.*, **23**, 3143 (1993).
[33] J.B. Flanagam, A.J. Bard, F. Canson. *J. Am. Chem. Soc.*, **100**, 4248 (1978).
[34] R.L. Lintvedt, L.S. Kramer. *Inorg. Chem.*, **22**, 796 (1983).
[35] F.D. Earl, R.L. Lintvedt. *J. Am. Chem. Soc.*, **100**, 6367 (1978).
[36] P. Zanello, S. Tamburini, P.A. Vigato, G.A. Mazzocchin. *Coord. Chem. Rev.*, **77**, 165 (1987).
[37] E.Q. Gao, W.M. Bu, G.M. Yaug, D.Z. Liao, Z.H. Jiang, S.P. Yan, G.L. Wang. *J. Chem. Soc., Dalton Trans.*, 1431 (2000).